High-resolution Al $L_{2,3}$-edge x-ray absorption near edge structure spectra of Al-containing crystals and glasses: coordination number and bonding information from edge components

2008 J. Phys.: Condens. Matter 20 135219

(http://iopscience.iop.org/0953-8984/20/13/135219)

IOP Publishing Journal of Physics: Condensed Matter

J. Phys.: Condens. Matter **20** (2008) 135219 (8pp) doi:10.1088/0953-8984/20/13/135219

High-resolution Al $L_{2,3}$-edge x-ray absorption near edge structure spectra of Al-containing crystals and glasses: coordination number and bonding information from edge components

C Weigel[1], G Calas[1], L Cormier[1], L Galoisy[1] and G S Henderson[2]

[1] Institut de Minéralogie et de Physique des Milieux Condensés, Université Pierre et Marie Curie, Université Paris Diderot, IPGP, CNRS UMR 7590, 4 place Jussieu, 75005 Paris, France
[2] Department of Geology, The University of Toronto, 22 Russell Street, Toronto, ON, M5S 3B1, Canada

Received 21 January 2008, in final form 21 February 2008
Published 13 March 2008
Online at stacks.iop.org/JPhysCM/20/135219

Abstract

High-resolution Al $L_{2,3}$-edge x-ray absorption near edge structure (XANES) spectra have been measured in selected materials containing aluminium in 4-, 5- and 6-coordination. A shift of 1.5 eV is observed between the onset of $^{[4]}$Al and $^{[6]}$Al $L_{2,3}$-edge XANES, in agreement with the magnitude of the shift observed at the Al K-edge. The differences in the position and shape of low-energy components of Al $L_{2,3}$-edge XANES spectra provide a unique fingerprint of the geometry of the Al site and of the nature of Al–O chemical bond. The high resolution allows the calculation of electronic parameters such as the spin–orbit coupling and exchange energy using intermediate coupling theory. The electron–hole exchange energy decreases in tetrahedral as compared to octahedral symmetry, in relation with the increased screening of the core hole in the former. Al $L_{2,3}$-edge XANES spectra confirm a major structural difference between glassy and crystalline $NaAlSi_2O_6$, with Al in 4- and 6-coordination, respectively, Al coordination remaining unchanged in $NaAl_{1-x}Fe_xSi_2O_6$ glasses, as Fe is substituted for Al.

(Some figures in this article are in colour only in the electronic version)

1. Introduction

Al-oxides and aluminosilicates form crystalline and glassy materials of major technological and geophysical importance. In glasses, Al crystal chemistry controls a broad range of physical and chemical properties, including insulating and optical properties, molar volume and mechanical and thermodynamic properties. Al may occupy sites with different coordination numbers (CN), 4, 5 or 6 (hereafter noted $^{[4]}$Al, $^{[5]}$Al and $^{[6]}$Al, respectively), having a major influence on the structural properties. In oxide glasses, Al coordination is of great interest as it controls the structure of the glassy network. For instance, the presence of $^{[4]}$Al increases the polymerization of the glass structure due to the network-forming role of this Al CN [1].

Determining Al CN in multicomponent glasses requires the chemical resolution of spectroscopic techniques such as nuclear magnetic resonance (NMR), extended x-ray absorption fine structure (EXAFS), x-ray absorption near edge structure (XANES) and electron energy loss near edge structure (ELNES). EXAFS provides access to interatomic distances and cation CNs although disorder effects and site mixing limit its accuracy [2]. XANES and ELNES are also widely used to determine the chemical state and local stereochemical environment of cations, including bonding, valence, coordination, and site symmetry [2–5]. In addition, XANES and ELNES spectra are the projection of the atom-resolved, partial density of unoccupied states of the conduction band, which yields information on thermodynamic properties and, more generally, on phase stability. Indeed,

in aluminosilicates, Al–O and Si–O bonds involve the lowest unoccupied molecular orbitals of Si and Al and the highest-occupied molecular orbitals of O [6–8]. Due to limited broadening resulting from long core–hole lifetimes [9], $L_{2,3}$-edge XANES spectra show an increased spectral definition compared with K-edge spectra.

Within single-electron theory, the dominant absorption features of $L_{2,3}$-edge XANES spectra are described through excitation of a 2p electron to unoccupied s- and d-like density of states. The excitation energy lies in the band gap and is therefore interpreted in terms of exciton absorption, the Al 3s levels being pulled down into the band gap from the bottom of the conduction bands by the core–hole potential [10–12]. The onset energies correspond to transitions to the lowest unoccupied s-like states [13], modified by the core–hole potential. The absorption edge is split by spin–orbit coupling. This yields a separation of the 2p core state into $2p_{3/2}$ ($j = 3/2$) and $2p_{1/2}$ ($j = 1/2$) core levels, which correspond to L_3 and L_2 edges, respectively. High-resolution synchrotron radiation XANES spectroscopy reaches spectral resolutions of 0.03 eV. It is then possible to resolve fine features such as the L_2 and L_3 excitons at the Al $L_{2,3}$-edge. As the energy width of spectral features is inversely related to the lifetime of the excited state, spectra tend to be narrower in insulators (e.g. α-Al_2O_3) than in metals, in which deep core levels tend to exhibit short lifetimes. Hence, $L_{2,3}$-edge XANES allows detailed investigation of the s- and d-like levels, which are important for understanding the nature of the Al–O bond in insulating samples, such as the ones studied here. However, despite this interest and the need for high-resolution spectra for helping in the interpretation of ELNES features, there are no data showing how Al $L_{2,3}$-edge XANES spectra vary as a function of crystal structure and composition.

We present high-resolution Al $L_{2,3}$-edge XANES spectra of crystalline materials containing different Al CN's. These crystalline references include α-Al_2O_3 (corundum), $NaAlSi_2O_6$ (jadeite), $NaAlSi_3O_8$ (albite), $NaAlSiO_4$ (nepheline), $AlPO_4$ (berlinite) and the Al_2SiO_5 polymorphs (kyanite, sillimanite, andalusite). This reference dataset is used to investigate the local structure of $NaAl_{1-x}Fe_xSi_2O_6$ glasses, a system in which magnetic properties preclude the use of magnetic resonance techniques to determine the surrounding of Al atoms. Taking advantage of the information provided by our high instrumental resolution, focus has been given to the variations in edge shape and position of the low-energy edge components of the Al $L_{2,3}$-edge XANES spectra. These variations confirm the strong influence of Al site geometry and the spectral resolution allows us to clearly resolve the L_3 and L_2 edges. This additional information allows quantification of spin–orbit coupling values and exchange energy, as well as the relative contribution of the L_2 and L_3 edges to the overall XANES features. Variation of these parameters is responsible for the observed differences of the XANES spectra between the different compounds investigated. Low-energy components of Al $L_{2,3}$-edge XANES spectra provide a unique fingerprint of the Al-surrounding, in contrast to the broad components located at higher energy and/or related to multiple scattering, which are widely used in ELNES [14]. Al $L_{2,3}$-edge XANES spectra show that Al retains a network-forming position in $NaAl_xFe_{1-x}Si_2O_6$ glasses during the Al to Fe substitution. As our knowledge of glass structure is generally limited by disorder effects, Al $L_{2,3}$-edge XANES provides interesting complementary information on the surrounding of Al in glasses.

Table 1. Composition and usual name for the crystals, atomic content of Al, coordination number of Al, average Al–O distances and site multiplicity.

Sample	Composition	at.% Al	CN_{Al-O}	Average d_{Al-O} (Å) and site multiplicity
Corundum[a]	α-Al_2O_3	40.0	6	1.914
Jadeite[b]	$NaAlSi_2O_6$	20.0	6	1.928
Kyanite[c]	k-Al_2SiO_5	33.3	6	1.907 (4 sites)
Andalusite[c]	a-Al_2SiO_5	33.3	5	1.836 (2 sites)
			6	1.935 (2 sites)
Sillimanite[c]	s-Al_2SiO_5	33.3	4	1.764 (2 sites)
			6	1.912 (2 sites)
Berlinite[d]	$AlPO_4$	33.3	4	1.738
Low albite[e]	$NaAlSi_3O_8$	7.7	4	1.742
Nepheline[f]	$NaAlSiO_4$	14.3	4	1.719

[a] Reference [15].
[b] Reference [16].
[c] Reference [17].
[d] Reference [18].
[e] Reference [19].
[f] Reference [20].

2. Experimental details

The crystalline model compounds used in this study are presented in table 1 along with details on the Al crystal chemistry. The model compounds include α-Al_2O_3 and a chain silicate (jadeite-$NaAlSi_2O_6$) for $^{[6]}$Al, and $AlPO_4$ (berlinite) and two framework silicates (albite-$NaAlSi_3O_8$, nepheline-$NaAlSiO_4$) for $^{[4]}$Al. Furthermore, we also investigated the Al_2SiO_5 polymorphs, sillimanite (s-Al_2SiO_5), andalusite (a-Al_2SiO_5), and kyanite (k-Al_2SiO_5), in which Al occupies two distinct crystallographic sites. One site contains Al in 6-fold coordination while the other has Al in 4- (sillimanite), 5- (andalusite) or 6-fold coordination (kyanite). The identification of all samples was confirmed by powder x-ray diffraction.

Absorption experiments were performed at the Canadian Light Source (CLS) (Saskatoon, Canada) on the Variable Line Spacing Plane Grating Monochromator (VLS PGM) beamline. This beamline uses a 185 mm planar undulator, and three variable line spacing gratings to cover a photon energy of 2.5–250 eV. The medium energy grating was used in this study and accesses energies from 25 to 120 eV. The entrance and exit slits were set at 50 μm, giving a flux of about 10^{12} photons/s/100 mA and a resolution ($E/\Delta E$) greater than 10 000 at 100 eV [21]. The spectra were normalized to the intensity of the incident beam (I_0), which was determined from monitoring the current emitted from a nickel mesh located after the last focussing mirror. Photon energy was calibrated against Kr 3d and Ar 2p lines [22] and the energy stability of the beamline is better than 0.04 eV between different sample runs. XANES spectra were recorded simultaneously in fluorescence yield (FLY) and total electron yield (TEY) modes. A microchannel-plate detector was used to record the

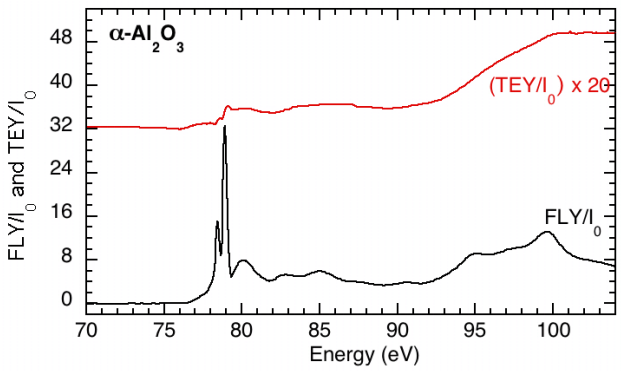

Figure 1. Comparison of TEY and FLY spectra normalized to I_0 for α-Al_2O_3. TEY has been multiplied by 20 for clarity.

FLY spectra while TEY spectra were recorded by measuring the sample current as a result of the photoabsorption.

Sample preparation consisted of grinding the samples to a fine powder and depositing them on carbon tape supported on a stainless steel sample holder. Prior to each experiment, the samples were dehydrated for one hour in an oven at 100 °C and then placed in the sample chamber. Three spectra were obtained for each sample and then averaged. We did not observe any incident beam damage on the samples. The spectra were normalized to the intensity of the incident beam, I_0 and a linear fit of the pre-edge background was subtracted. In addition each spectrum has been normalized to the peak with maximum intensity in order to aid in comparison of the data. The position of the edge components was determined by their apparent maximum.

3. Results

The edge onset at the Al $L_{2,3}$-edge corresponds to atomic-like excitations, which have been modified by the coordination state of the Al and the nature of the chemical bonding. We therefore focus on the XANES features observed near the edge onset, for which the enhanced spectral resolution clearly resolves the L_2 and L_3 edges split by the spin–orbit coupling.

As shown in figure 1, the Al $L_{2,3}$-edge XANES spectra of the investigated compounds are rich in structure. The high resolution attained is essential to characterize accurately the various edge features. The FLY and TEY spectra exhibit similar edge shapes but the detailed spectral features are more clearly resolved in the FLY spectra (figure 1). Indeed, spectra collected in TEY mode are surface sensitive and, for insulating samples like those investigated here, are affected by surface charging. The XANES spectrum of α-Al_2O_3 is in good agreement with previous studies [23], but the higher spectral resolution provides a better separation of the L_2 and L_3 edges. The experimental Al $L_{2,3}$ XANES spectra at the vicinity of the absorption threshold for $^{[4]}$Al, $^{[5]}$Al and $^{[6]}$Al are shown in figure 2. They exhibit variations in position, shape and relative intensity of the low-energy components (labelled A and B following previous conventions [24]). Several absorption peaks exist in this energy region, with feature A

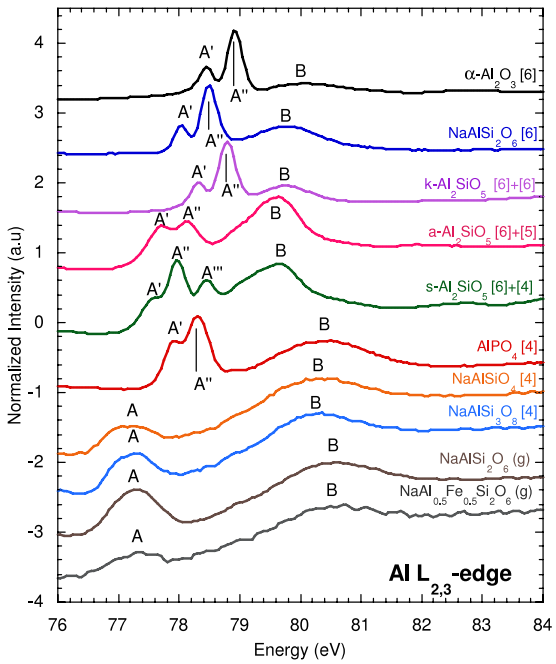

Figure 2. XANES Al $L_{2,3}$-edge spectra of crystals and glasses (the numbers in brackets indicate the Al CN. The glasses are indicated by (g)).

being resolved into two or more components (A′, A″ and sometimes A‴) in most spectra. The variation in the relative intensity of features A and B is due to the selection rules for the different symmetries but site distortion significantly contributes to enhance the intensity of peak B [25]. In addition, the edges shift to lower energy as Al coordination decreases. The shift of the edge onset between $^{[4]}$Al and $^{[6]}$Al is ∼1.5 eV (table 2), a value similar to that observed at the Si $L_{2,3}$-edge between $^{[6]}$Si and $^{[4]}$Si in crystals and glasses [26, 27]. The intensity of the two main components at the absorption edge is different for 4- and 6-coordinated Al, due to differences between Al site symmetry, as noted above.

In the samples with Al exclusively in octahedral coordination (α-Al_2O_3, $NaAlSi_2O_6$ and k-Al_2SiO_5), Al $L_{2,3}$ XANES spectra exhibit similar shapes but with individual spectral features occurring at different energies. Peak A has the strongest intensity and has two clearly resolved components (A′ and A″), with similar relative intensities, the A′ component being the less intense. The A′ and A″ components corresponds to the L_3 and L_2 edges, respectively. The full width at half maximum (FWHM) of the individual edge (A′ and A″) components are similar in samples that contain edge sharing AlO_6 octahedra ($NaAlSi_2O_6$, Al_2SiO_5 polymorphs and Al_2O_3), despite differences in Al site multiplicity and point group symmetry.

$^{[4]}$Al has been investigated in two framework aluminosilicates ($NaAlSi_3O_8$, $NaAlSiO_4$) and in $AlPO_4$, which is isostructural with α-quartz (SiO_2). The $L_{2,3}$-edge XANES spectra of the two aluminosilicates containing $^{[4]}$Al exhibit similar features, which are shifted to lower energy than in the XANES spectra of phases containing $^{[6]}$Al. In these compounds, the L_3 and L_2 edges are not resolved and peak B is the most intense

Table 2. Position of the XANES features A, B and C, spin–orbit splitting calculated with the position of the L_2 and L_3. The peak positions are determined at the maximum. The estimated uncertainty on the peak position is ±0.02 eV.

	A (eV)					
Sample	A′ (eV)	A″ (eV)	B (eV)	Spin–orbit splitting ξ (eV)	Binding energy (eV)	Onset energy (eV)
α-Al_2O_3	78.45	78.92	80.11	0.47	74.48[a]	77.9
$NaAlSi_2O_6$	78.03	78.49	79.79	0.46	—	77.7
k-Al_2SiO_5	78.31	78.79	79.77	0.48	74.48[a]	77.8
a-Al_2SiO_5	77.72 and 78.13		79.64 (and 78.95)	∼0.41	74.07[a]	76.9
s-Al_2SiO_5	77.60, 77.97 and 78.45		79.65	0.37 and 0.48	74.65[a], 74.06[a]	77.0
$AlPO_4$	77.92	78.30	80.45	0.38	75.0[b]	77.4
$NaAlSi_3O_8$	77.32		80.3	∼0.42	74.3[c]	76.5
$NaAlSiO_4$	77.16		80.3	∼0.37	—	76.4
$NaAlSi_2O_6$ (g)	77.30		80.3	<0.4	—	76.4
$NaFe_{0.5}Al_{0.5}Si_2O_6$ (g)	77.32		80.3	<0.4	—	76.4

[a] Reference [44].
[b] Reference [45].
[c] Reference [46].

feature near the absorption threshold (figure 2). The topological environment around Al is distributed in $NaAlSi_3O_8$ and $NaAlSiO_4$, due to the existence of four distinct tetrahedral sites together with a distribution in the nature of the Al next nearest neighbours (NNN). The resulting broadening of the edge components is at the origin of the merging of the L_3 and L_2 edges into one broad feature as also observed in $MgAl_2O_4$ [11]. The splitting of the A feature can be evaluated by curve fitting the spectral envelope with two Gaussian components and the results of the fits are given in table 2. This Gaussian line shape indicates chemical and structural disorder, at the origin of a large number of local topological configurations. As observed in an Al $L_{2,3}$-edge ELNES investigation of anorthite, the sensitivity of low-energy spectra to the structure beyond the coordination shell results in a loss of spectral resolution [28]. The edge onset of the $AlPO_4$ XANES spectrum is shifted to higher energy relative to the framework aluminosilicates and the features of peak A are better resolved, although with a smaller separation between A′ and A″ components than in the spectra of $^{[6]}$Al (table 2). In addition, the A′ feature is less intense than A″, but with a higher relative intensity (A′/A″) than in the spectra of $^{[6]}$Al.

Site mixing effects have been investigated using s-Al_2SiO_5 and a-Al_2SiO_5, in which $^{[6]}$Al coexists with $^{[4]}$Al or $^{[5]}$Al, respectively. The $L_{2,3}$-edge ELNES spectra are different among the Al_2SiO_5 polymorphs [25], but the enhanced resolution of the XANES spectra allows us to better understand the relative contribution of the different Al CNs to the overall spectral features. In s-Al_2SiO_5, with Al in 4- and 6-coordination, there are three features at 77.60 eV (A′), 77.97 eV (A″) and 78.45 eV (A‴). The feature A′, at the lowest energy is assigned to the L_3-edge of $^{[4]}$Al due to the low-energy position of the feature. The position of the structure at the highest energy is in agreement with the position of the L_2-edge of $NaAlSi_2O_6$ and is therefore assigned to the L_2-edge of $^{[6]}$Al. Consequently, the intermediate feature A′, is the superposition of the L_2-edge of $^{[4]}$Al and the L_3-edge of $^{[6]}$Al. The XANES of a-Al_2SiO_5, with $^{[5]}$Al and $^{[6]}$Al, also shows two features contributing to the A component, at 77.72 and 78.13 eV. The shift to lower energy observed from k- to a- and s-Al_2SiO_5 can be correlated with a progressive decrease of the nominal charge (expressed in valence units, v.u.) on O, calculated on the basis of Pauling electrostatic bond valence principle [29]: −2, −1.98 and −1.94 v.u., for k-, a- and s-Al_2SiO_5 respectively.

Peak B occurs at higher energy in the compounds containing $^{[4]}$Al relative to that of compounds containing only $^{[6]}$Al. However, in the compounds containing different Al coordination sites (a- and k-Al_2SiO_5), it occurs at the same position, but is more intense and asymmetrical in a-Al_2SiO_5. In s-Al_2SiO_5, which contains Al in 6- and 4-fold sites, there is an additional broad B component at higher energy. This high-energy component is at the same position as peak B in the spectra of compounds that contain exclusively $^{[4]}$Al and is probably associated with the $^{[4]}$Al site. However, this peak occurs at a different position (relative to the peak A) in $AlPO_4$, despite similar Al–O distances to those found in $NaAlSi_3O_8$ and $NaAlSiO_4$. This feature does not correspond to multiple scattering events, characterized by a dependence of the peak position as a function of cation–oxygen distances [4], which is not observed for peak B. In tetrahedral symmetry, its high intensity with respect to the A feature arises from s–p hybridization. Furthermore, even in octahedral symmetry, site distortion intensifies this feature, because of the increased s-character of the final state, as shown by the comparison between α-Al_2O_3 and the aluminosilicates.

There is a strong difference between the spectra of crystalline and amorphous $NaAlSi_2O_6$. The edge threshold is shifted in the glass to lower energy than in the $NaAlSi_2O_6$ crystalline phase, which contains $^{[6]}$Al but is at the same energy position as in the $NaAlSiO_4$ and $NaAlSi_3O_8$ crystalline phases where Al is exclusively $^{[4]}$Al. This indicates a major structural difference between glassy and crystalline $NaAlSi_2O_6$, a confirmation of previous NMR studies, which showed that Al is 4-coordinated in $NaAlSi_2O_6$ glass, with AlO_4 tetrahedra randomly distributed throughout the silicate network [30]. Furthermore, the edge onset observed on the spectra of the glasses is not at the same position as in the spectra of the crystalline phases that contain $^{[5]}$Al

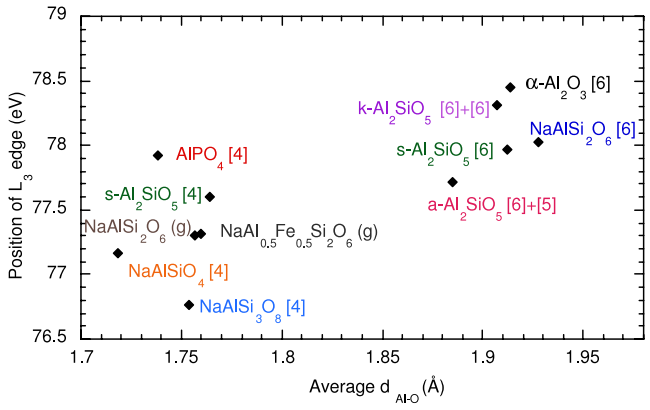

Figure 3. Correlation between the position of L_3 maximum and the average Al–O distances. The coordination number of Al is indicated for the crystalline references. This relationship shows the presence of $^{[4]}$Al in the glasses (indicated as (g)).

(a-Al_2SiO_5) and $^{[6]}$Al, which excludes the presence of a significant proportion of $^{[5]}$Al and $^{[6]}$Al.

The overall XANES spectra are similar in $NaAl_{1-x}Fe_xSi_2O_6$ glasses. However, only the spectra of the glasses with $x < 0.5$ have an acceptable signal-to-noise ratio. Peak A is broad and unresolved by comparison with spectra obtained on crystalline phases. This broadening is caused by the increased distribution of bond distances and angles resulting from the disordered nature of the glassy structure. The position of the XANES features does not change in the glasses ($NaAl_{1-x}Fe_xSi_2O_6$) indicating that Al retains the same CN throughout the Al–Fe substitution range.

4. Discussion

4.1. Influence of the Al site

In figure 3, the position of the L_3 peak maximum is plotted against the average Al–O distance for each site in the different compounds investigated. For $NaAlSi_2O_6$ and $NaAl_{1-x}Fe_xSi_2O_6$ glasses, the Al–O distance was obtained by a Gaussian fit of neutron diffraction correlation functions [31]. The L_3-edge position for $^{[4]}$Al-containing compounds occurs at lower energy than for $^{[6]}$Al-containing compounds. The differences in the spectra of the phases containing $^{[4]}$Al or $^{[6]}$Al result from the strong p–d hybridization allowed for Td symmetry but forbidden for Oh symmetry [13]. Additional differences between the electronic structures of $^{[4]}$Al and $^{[6]}$Al result from the presence of a core hole in the final state, which affects the absorption spectra by creating an attractive potential that shifts the edge toward lower energy. In Oh symmetry, the core–hole is screened by a charge transfer from O to Al, which is not allowed in Td symmetry. The screening is therefore more important for octahedral than for tetrahedral symmetry [13]. The position of the L_3-edge in a-Al_2SiO_5, with $^{[5]}$Al and $^{[6]}$Al, is between that of $^{[4]}$Al and $^{[6]}$Al. In a compound of unknown Al CN, Al $L_{2,3}$-edge XANES is thus an attractive probe to determine Al CN. For $^{[4]}$Al-compounds, the more distributed environment around Al, arising from site multiplicity and from the distribution of the nature of the NNN's, is responsible for the merging of the L_3 and L_2 edges into one broad feature A, as mentioned previously. By contrast, the presence in $AlPO_4$ of only one Al site, slightly distorted (Al–O distance distribution of 0.01 Å) results in the resolution of L_2 and L_3 edges. In glasses, no edge onset shift is observed relative to crystals with $^{[4]}$Al. Al keeps a tetrahedral coordination in the $NaAl_{1-x}Fe_xSi_2O_6$ glasses for the x values investigated, charge compensation being ensured by Na, which gives a continuous random network with all oxygens in bridging configurations and Si and Al both in tetrahedral coordination, such as in other aluminosilicate glasses in which the modifier oxide/Al_2O_3 ratio $R = 1$ [1]. The low packing efficiency results in a density decrease from crystalline to glassy $NaAlSi_2O_6$, 3.2 and 2.3, respectively [31].

4.2. Nature of bonds and position of the threshold

The position of the $L_{2,3}$-edge is sensitive to the nature of the chemical bond, which depends for a given site geometry on the nature of the Al NNN. Then, second and further nearest neighbours have an influence on the $L_{2,3}$-edge spectra even though they are not probed directly [5, 28]. The position of the edge onset is related to the effective charge on the Al atoms in the different materials. The more ionic the bonds, the higher the energy of the threshold. Indeed, Al_2O_3 is the most ionic of all compounds studied in this work and its threshold appears at the highest energy. Furthermore, as the Al NNNs include Si such as in the Al_2SiO_5 polymorphs, the edge onset is shifted to lower energy relative to Al_2O_3. This reflects the effect of the next nearest Si neighbours, the presence of which decreases the effective charge of the O neighbours, producing a shift of the lowest unoccupied Al s states to lower energy. For the $^{[6]}$Al-containing crystals, the edge onset is also located at low energy in the presence of alkalis (such as in $NaAlSi_2O_6$), due to the smaller polarizability of alkalis. The influence of the polarizing power of the NNN has also been observed at Si $L_{2,3}$-edges in various crystals, where silicates with the least polarizing NNN cations, e.g., Ca, Mg, and Fe, have low-energy edge onsets relative to α-quartz [5].

For $^{[4]}$Al reference compounds, the threshold is shifted to lower energy in aluminosilicates, as compared to $AlPO_4$. This shift of the threshold towards higher energy in $AlPO_4$ is due to the presence of P as the NNN. As a consequence the Al–O bond has little charge density between the atoms and has a clear ionic character [32]. In aluminosilicates $NaAlSi_3O_8$ and $NaAlSiO_4$, the Al NNNs are Si and Al, and there is a higher charge density shared on the Al–O bonds, due to the more similar bonding around O atoms.

In glasses, no edge onset shift is observed compared to crystals with the same Al CN. In addition, the edge onset does not appear to shift in the presence of Fe, which indicates that Fe sites are not linked with Al sites in these glasses. In contrast, the Si $L_{2,3}$-edge onset shifts to lower energy in presence of Fe NNN around Si and a shift is also observed in the spectra of crystals relative to their amorphous equivalents [5]. This shift is attributed to the lowering of the conduction-band edge onset or to the high density of localized band-tail states in the

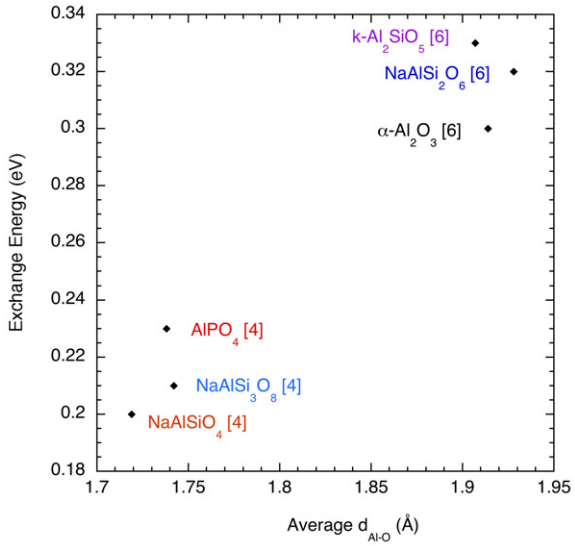

Figure 4. Variation of exchange energy Δ as a function of the average Al–O distance. The two Al CNs are clearly distinguished by this parameter.

forbidden gap [33]. The more ionic nature of the Al–O bond relative to the Si–O bond explains the absence of shift in the Al $L_{2,3}$-edge between crystalline and amorphous aluminosilicates.

Spin–orbit coupling values may be deduced from the splitting between L_2 and L_3 components (table 2). The magnitude of spin–orbit splitting decreases with distance from nucleus and hence with Al–O covalence, due to increased nuclear shielding. In Al silicates, $^{[4]}$Al and $^{[6]}$Al correspond to a spin–orbit splitting of ∼0.39 eV and 0.47 eV, respectively and consequently the spin–orbit coupling values can be used to discriminate differences in Al–CN. In the glasses investigated, peak A is broad and the L_2 and L_3 edges are unresolved, which corresponds to a maximum spin–orbit coupling value of ∼0.4 eV, consistent with the presence of $^{[4]}$Al.

4.3. Variations of the exchange energy

The relative intensity of the L_3 and L_2 components, $I(L_3)/I(L_2)$, was evaluated by taking the absolute intensity of the L_3 and L_2 peaks relative to a horizontal background set at zero. $I(L_3)/I(L_2)$ is equal to 0.64 ± 0.03 for $^{[4]}$Al versus 0.43 ± 0.03 for $^{[6]}$Al. This observation combined with the smaller spin–orbit coupling values for $^{[4]}$Al explains the fact that L_3 and L_2 edges have merged in $NaAlSi_3O_8$ and in $NaAlSiO_4$.

The difference in $I(L_3)/I(L_2)$ between $^{[4]}$Al and $^{[6]}$Al can be understood within the intermediate coupling theory in terms of screening of the core hole. Increased screening reduces the exchange energy, which represents the attraction between the core hole and the photoelectron. With an infinite separation between the core hole and the photoelectron, the electron–hole exchange energy Δ would be equal to zero and the $L_{2,3}$ spin–orbit splitting ξ would be much larger than Δ. A statistical value of 2/1 is then predicted for the $I(L_3)/I(L_2)$ value. Because the screening is more important in Oh than in Td symmetry [13], the $I(L_3)/I(L_2)$ ratio should be closer to 2/1 for octahedral than for tetrahedral environment. But variations in the relative values of the exchange energy and spin–orbit splitting modify the actual $I(L_3)/I(L_2)$ values [12]. In tetrahedral symmetry, the difference observed between $AlPO_4$ and the aluminosilicates arises from the electronegativity of Al NNN, P and Si, with electronegativity being higher in the former compared to the latter. $I(L_3)/I(L_2)$ can be used to determine the electron–hole exchange energy Δ between the core hole and the bound photoelectron. As demonstrated by Onodera and Toyosawa [34] and by Balzarotti *et al* [10] for the electronic transition $p^6 \rightarrow p^5s$ [34], the exchange energy is calculated from the following relationship, assuming that ξ and Δ are of similar magnitude:

$$I(L_3)/I(L_2) = \tan^2\left[\arctan 2^{1/2} - \frac{1}{2}\arctan\left(\frac{8^{1/2}\Delta}{3\xi - \Delta}\right)\right]. \quad (1)$$

The $L_{2,3}$ spin–orbit splitting ξ value has been fixed at the free ion value, 0.426 eV [12]. The Δ values of the crystalline reference compounds have been calculated within the intermediate coupling theory (table 3). The value for α-Al_2O_3 is similar to that previously determined [12]. Δ is smaller by about 0.1 eV for $^{[4]}$Al than for $^{[6]}$Al (figure 4), due to the weaker core–hole screening of Al in Td symmetry [13]. The small dispersion of the exchange energy shows that this parameter is a useful indicator of Al coordination.

Table 3. Estimation of L_3/L_2 intensity and exchange energy for reference compounds.

Sample	CN_{Al-O}	L_3/L_2 intensity	Exchange energy Δ (eV)
α-Al_2O_3	6	0.46	0.30
$NaAlSi_2O_6$	6	0.43	0.32
k-Al_2SiO_5	6 + 6	0.40	0.33
$AlPO_4$	4	0.64	0.23
$NaAlSi_3O_8$	4	0.71	0.21
$NaAlSiO_4$	4	0.76	0.20

4.4. Comparison with Al K-edge XANES

In a traditional interpretation of the XANES/ELNES spectra, the K-edge of an atom corresponds to the p component of the local density of states of the atom in the conduction band, while the $L_{2,3}$-edge corresponds to the (s + d) component. In Al K-edge XANES, the different Al CNs are distinguished by the specific position and relative intensity of the edge components [35–37]. In both K- and $L_{2,3}$ XANES spectra, the edge onset of $^{[6]}$Al shifts by ∼1.5–2 eV to higher energy compared to that of $^{[4]}$Al. A common energy scale may be used to compare the two kinds of XANES spectra (figure 5), aligning the pre-edge feature in Al K-edge XANES (assigned to s-like final states with some p-character due to site distortion) with peak A in the $L_{2,3}$-edge XANES (assigned to an s–p–d hybridized orbital) [13]. Both the K- and L-edge XANES spectra discriminate Al in different coordination environments, but the differences induced by different Al CNs are more pronounced at the Al $L_{2,3}$-edge than at the K-edge. The Al $L_{2,3}$-edge is sensitive to the

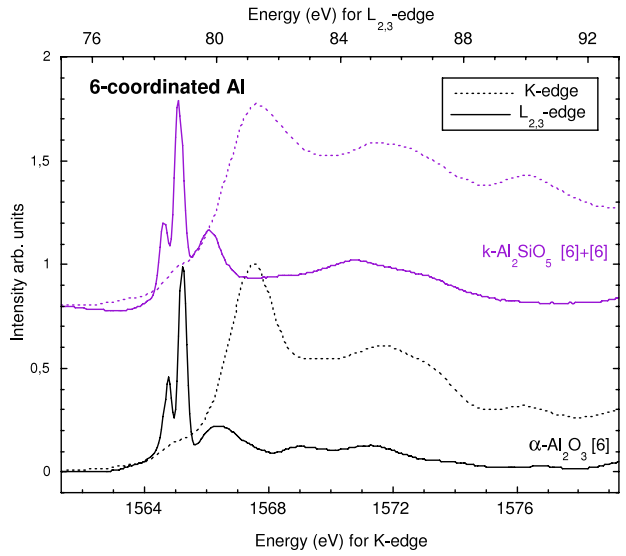

Figure 5. Al $L_{2,3}$- and K-edges of $^{[6]}$Al reference compounds. The energy scales at the top and at the bottom are for $L_{2,3}$- and K-edges, respectively.

short-range structure and electronic environment of the Al. For example, the overall shape of the Si $L_{2,3}$-edge XANES spectrum on quartz SiO_2 is reproduced by *ab initio* full MS calculations, using a 5-atom model [38]. This indicates that information in $L_{2,3}$ spectra concerns mainly short-range interactions. This is different for the Al K-edge XANES spectra that are sensitive to structural ordering up to 15 Å around the absorbing aluminium atom [39]. That the medium-range ordering is less important in $L_{2,3}$-edge than in K-edge spectra is interpreted to be due to the decreased hybridization of the s and d orbitals; the s orbital density sampled at the $L_{2,3}$-edge is more local [13]. Consequently, Al $L_{2,3}$-edge XANES provides more information on local structural changes, while the splitting of the L_3 and L_2 edge gives information on the electronic state.

4.5. Core hole influence on transition energy

During x-ray absorption, the excitation of a photoelectron creates a core hole, which modifies the energy of the final state. The effective energy difference between the initial-state and the final-state energy levels is given by $\Delta E = h\nu + U$, where $h\nu$ is the photon energy, and U the core–hole-photoelectron attraction [13]. The larger screening in Oh than in Td symmetry modifies the U values, which contributes to the shift of the XANES features observed for $^{[4]}$Al and $^{[6]}$Al. The difference between the Al $L_{2,3}$-edge onsets and the Al 2p binding energies (BE) varies between 2.2 and 3.4 eV in the compounds investigated (table 2). The former is a measure of the energy required to promote the 2p core electron to the lowest unoccupied Al s-like state above the Fermi level. The latter corresponds to the energy of the 2p core electron relative to the Fermi level [40]. In insulating oxides and silicates, the Fermi level is located in the middle of the band gap and the differences between the Al $L_{2,3}$-edge onsets and Al 2p BEs should be equal to half of the band-gap energies. The band gap evaluated here for $^{[4]}$Al and $^{[6]}$Al is about 4.5 and 7 eV, respectively. The band gap for $^{[4]}$Al is the same as derived for $^{[4]}$Si. For $^{[6]}$Al, the value is smaller than the optical band gap, 8.9 eV [41]. The resulting band-gap values underestimate significantly the actual values in these wide-band-gap insulators, as observed in silicates [33]. In these compounds, the presence of a core hole pulls down the ground state conduction-band onset during the absorption process [42, 43]. The relative position of both the initial core level and the unoccupied final state is affected by the charge transfer occurring as a result of chemical bonding. The smaller band gap of $^{[6]}$Al is an indication of a smaller charge transfer due to a more ionic Al–O bond.

5. Conclusion

Low-energy components of Al $L_{2,3}$-edge XANES spectra provide unique information not only on CNs but also on the nature of chemical bonding and the geometry of Al site. They may be used as a comparison dataset for future ELNES investigations of Al compounds. Comparison of the XANES spectra of crystalline reference compounds containing 6-, 5- and 4-coordinated Al confirms the strong influence of Al site geometry. A shift of 1.5 eV is observed between the onset of the $L_{2,3}$-edge XANES spectra of $^{[4]}$Al and $^{[6]}$Al, in agreement with the magnitude of the shift observed between these two CNs at the Al K-edge. The two kinds of information obtained from K- and $L_{2,3}$-edge XANES spectra are complementary because of their different selection rules. The variations of the spin–orbit coupling and of the exchange energy are responsible for the observed differences of the XANES spectra between the different compounds investigated. This study confirms that the exchange energy, calculated using the intermediate coupling theory, decreases in tetrahedral versus octahedral symmetry, in relation with an increased screening of the core–hole in the former. Al $L_{2,3}$-edge XANES spectra confirm a major structural difference between glassy and crystalline $NaAlSi_2O_6$, with Al in 4- and 6-coordination, respectively. We show that Al retains a network-forming position in $NaAl_{1-x}Fe_xSi_2O_6$ glasses during Fe–Al substitution. This gives rise to a continuous random network, explaining the density decrease from crystalline to glassy $NaAlSi_2O_6$, 3.2 and 2.2, respectively. As the knowledge of glass structure is often limited by disorder effects, $L_{2,3}$-edge XANES provides useful information to rationalize structure–property relationships in glasses.

Acknowledgments

The research described in this paper was performed at the Canadian Light Source (CLS), which is supported by NSERC, NRC, CIHR, and the University of Saskatchewan. We also want to thank Yongfeng Hu and Lucia Zuin for their support during the experiments on the VLS PGM beamline at the CLS. GSH acknowledges the support of NSERC in the form of a discovery grant. This is IPGP Contribution # 2348.

References

[1] Greaves G N and Sen S 2007 *Adv. Phys.* **56** 1
[2] Brown G E Jr, Calas G, Waychunas G A and Petiau J 1988 *Rev. Mineral.* **18** 431
[3] Calas G and Petiau J 1983 *Solid State Commun.* **48** 625
[4] Bianconi A, Fritsch E, Calas G and Petiau J 1985 *Phys. Rev.* B **32** 4292
[5] Garvie L A J and Buseck P 1999 *Am. Mineral.* **84** 946
[6] Gibbs G V, Downs J W and Boisen M B Jr 1994 *Rev. Mineral.* **29** 331
[7] Tossell J A 1975 *J. Am. Chem. Soc.* **97** 4840
[8] Tossell J A 1975 *J. Phys. Chem. Solids* **36** 1273
[9] Fister T T, Seidler G T, Rehr J J, Kas J J, Elam W T, Cross J O and Nagle K P 2007 *Phys. Rev.* B **75** 174106
[10] Balzarotti A, Antonangeli F, Girlanda R and Martino G 1982 *Solid State Commun.* **44** 275
[11] O'Brien W L, Jia J, Dong Q Y, Callcott T A, Mueller D R, Ederer D L and Kao C C 1993 *Phys. Rev.* B **47** 15482
[12] O'Brien W L, Jia J, Dong Q-Y, Callcott T A, Rubensson J-E, Mueller D L and Ederer D L 1991 *Phys. Rev.* B **44** 1013
[13] van Bokhoven J A, Nabi T, Sambe H, Ramaker D E and Koningsberger D C 2001 *J. Phys.: Condens. Matter* **13** 10247
[14] Bouchet D and Colliex C 2003 *Ultramicroscopy* **96** 139
[15] Finger L W and Hazen R M 1978 *J. Appl. Phys.* **49** 5823
[16] Prewitt C T and Burnham C W 1966 *Am. Mineral.* **51** 956
[17] Winter J K and Ghose S 1979 *Am. Mineral.* **64** 573
[18] Muraoka Y and Kihara K 1997 *Phys. Chem. Minerals* **24** 243
[19] Harlow G E and Brown G E Jr 1980 *Am. Mineral.* **65** 986
[20] Tait K T, Sokolova E, Hawthorne F C and Khomyakov A P 2003 *Can. Mineral.* **41** 61
[21] Reininger R, Tan K and Coulthard I 2002 *Rev. Sci. Instrum.* **73** 1489
[22] Hu Y F, Zuin L and Püttner R 2007 *Can. J. Chem.* **85** 1
[23] Chen J M, Simons J K, Tan K H and Rosenberg R A 1993 *Phys. Rev.* B **48** 10047
[24] Mo S-D and Ching W Y 2001 *Appl. Phys. Lett.* **78** 3809
[25] Hansen P L, Brydson R, McComb D W and Richardson I 1994 *Microsc. Microanal. Microstruct.* **5** 173
[26] Poe B T, Seifert F, Sharp T and Wu Z 1997 *Phys. Chem. Minerals* **24** 477
[27] Li D, Bancroft G M and Fleet M E 1996 *Am. Mineral.* **81** 111
[28] Jiang N, Qiu J and Spence J C H 2002 *Phys. Rev.* B **66** 054203
[29] Pauling L 1960 *The Nature of the Chemical Bond* (Ithaca, NY: Cornell University Press)
[30] Kohn S C, Dupree R, Mortuza M G and Henderson C M B 1991 *Am. Mineral.* **76** 309
[31] Weigel C, Cormier L, Calas G, Galoisy L and Bowron D T 2008 *J. Non-Cryst. Solids* submitted
[32] Christie D M, Troullier N and Chelikowsky J R 1996 *Solid State Commun.* **98** 923
[33] Garvie L A J, Rez P, Alvarez J R and Buseck P R 1998 *Solid State Commun.* **106** 303
[34] Onodera Y and Toyosawa Y 1967 *J. Phys. Soc. Jpn.* **22** 833
[35] Ildefonse P, Cabaret D, Sainctavit P, Calas G, Flank A-M and Lagarde P 1998 *Phys. Chem. Minerals* **25** 112
[36] Ildefonse P, Calas G, Flank A M and Lagarde P 1995 *Nucl. Instrum. Methods* B **97** 172
[37] Li D, Bancroft G M, Fleet M E, Feng X H and Pan Y 1995 *Am. Mineral.* **80** 432
[38] Wu Z Y, Jollet F and Seifert F 1998 *J. Phys.: Condens. Matter* **10** 8083
[39] Cabaret D, Sainctavit P, Ildefonse P and Flank A-M 1996 *J. Phys.: Condens. Matter* **8** 3691
[40] Hochella M F Jr 1988 *Rev. Mineral.* **18** 573
[41] Lazzari R and Jupille J 2001 *Surf. Sci.* **482** 823
[42] Brydson R 1996 *J. Phys. D: Appl. Phys.* **29** 1699
[43] Hamza S, Lewonczuk S, Ringeissen J, Beaurepaire E and Khan M A 1995 *Phys. Rev.* B **51** 17506
[44] Ohuchi F S, Ghose S, Engelhard M H and Baer D R 2006 *Am. Mineral.* **91** 740
[45] Benitez J J, Centeno M A, Odriozola J A, Conanec R, Marchand R and Laurent Y 1995 *Catal. Lett.* **34** 379
[46] Kyono A, Kimata M and Hatta T 2003 *Naturwissenschaften* **90** 414